ADVANCED OPTICAL MATERIALS

Supporting Information

for *Advanced Optical Materials*, DOI: 10.1002/adom.201900260

Arbitrary Manipulation of Light Intensity by Bilayer Aluminum Metasurfaces

Zhancheng Li, Wenwei Liu, Hua Cheng, Duk-Yong Choi, Shuqi Chen, and Jianguo Tian*

Supporting Information

Arbitrary Manipulation of Light Intensity by Bilayer Aluminum Metasurfaces

Zhancheng Li, Wenwei Liu, Hua Cheng, Duk-Yong Choi, Shuqi Chen and Jianguo Tian*

S1. The Wave-Transfer Matrix Method

The implementation of broadband polarization-selective transmission in the proposed bilayer metasurfaces is mainly attributed to the interference between the multiple reflections and the direct reflection. To verify this interpretation, we utilized the wave-transfer matrix method to make an analysis.[S1-S3] For a planar interface between two media *i* and *j* (whether with or without a nano structures), the forward and backward propagating waves can be related by utilizing a 4×4 wave-transfer Matrix $\mathbf{M}_{ji}$ while a 4×4 propagation matrix $\mathbf{P}_i$ can be used for a homogeneous medium *i*. The forward and backward propagating waves at the two ends of a multilayered medium can be related by the overall wave-transfer matrix **M** of the multilayered medium that can be treated as the matrix product of each part: $\mathbf{M}=\mathbf{M}_n\cdots\mathbf{M}_2\mathbf{M}_1$, where the element *1,2,…,N* are numbered along the wave propagating direction. For the proposed bilayer metasurfaces, the overall wave-transfer matrix **M** can be expressed as: $\mathbf{M}=\mathbf{M}_{dc}\mathbf{P}_c\mathbf{M}_{cb}\mathbf{P}_b\mathbf{M}_{ba}$, as shown in Figure S1(a). We simulated the coefficients of the scattering matrix $\mathbf{S}_{ji}$ of each interface firstly, and then we calculated the corresponding wave-transfer matrix $\mathbf{M}_{ji}$. Finally, we calculated the overall wave-transfer matrix **M** of the proposed bilayer metasurfaces, retrieved the coefficients of the overall scattering matrix **S** and calculated the transmission intensities. Figure S1(b) shows the simulated and calculated results of the modular square $t_{ij} = |T_{ij}|^2$ of the transmission coefficients T_{xx} and T_{yy}. Results show that the calculated results are in good agreement with the simulated one. The slight difference is owing to the neglecting of nanorod thickness that will introduced a tiny error in the

calculation of overall transfer matrix **M**. We also calculated the transmittance of the proposed bilayer metasurface under illumination with different polarization angles. As shown in Figure S1(c), the calculated results are also in good agreement with the simulated one (Figure 2b). Moreover, we also calculated the relationship between t_{xx} and the number of the nanorod layer, as shown in Figure S1(d). The results show that the working bandwidth is expanded dramatically in the proposed bilayer design compared to the single layer one and the working bandwidth can be further expanded with the increasing of the nanorod layer. It is worth mentioned that, even the working bandwidth can be further expanded with the increasing of the nanorod layer, the increasing percentage decrease dramatically. The further expanded of the working bandwidth can be realized by directly stacking two bilayer designs with adjacent working bandwidth instead of simply increasing the nanorod layer.

Supplementary figures

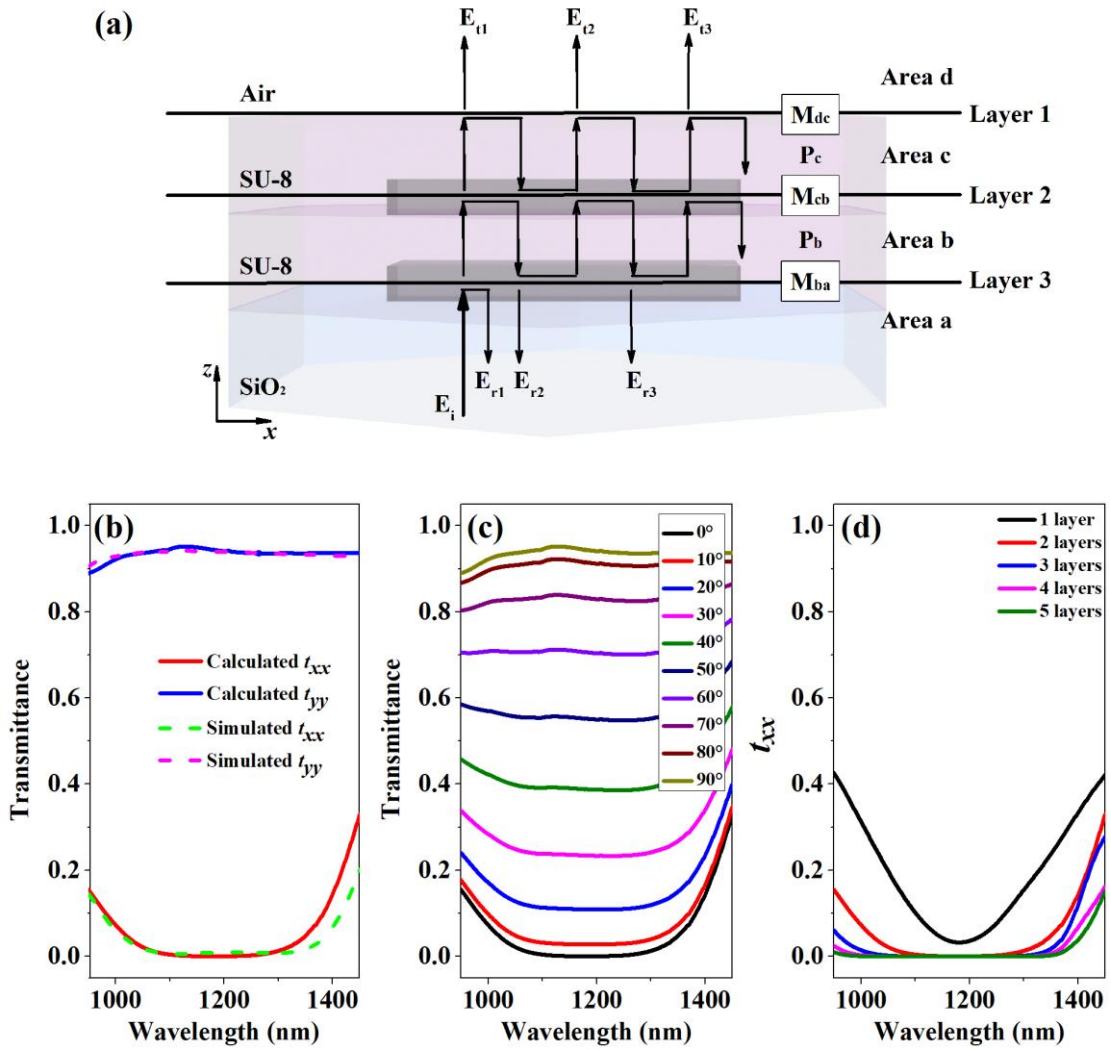

Figure S1. (a) Schematic of the multiple reflections in the proposed bilayer metasurfaces. (b) The simulated and calculated results of the modular square $t_{ij} = |T_{ij}|^2$ of the transmission coefficients T_{xx} and T_{yy}. (c) The calculated results of the transmittance under linearly polarized illumination with different polarization angles. (d) The calculated results of t_{xx} for metasurfaces with different numbers of nanorod layer (layer 2).

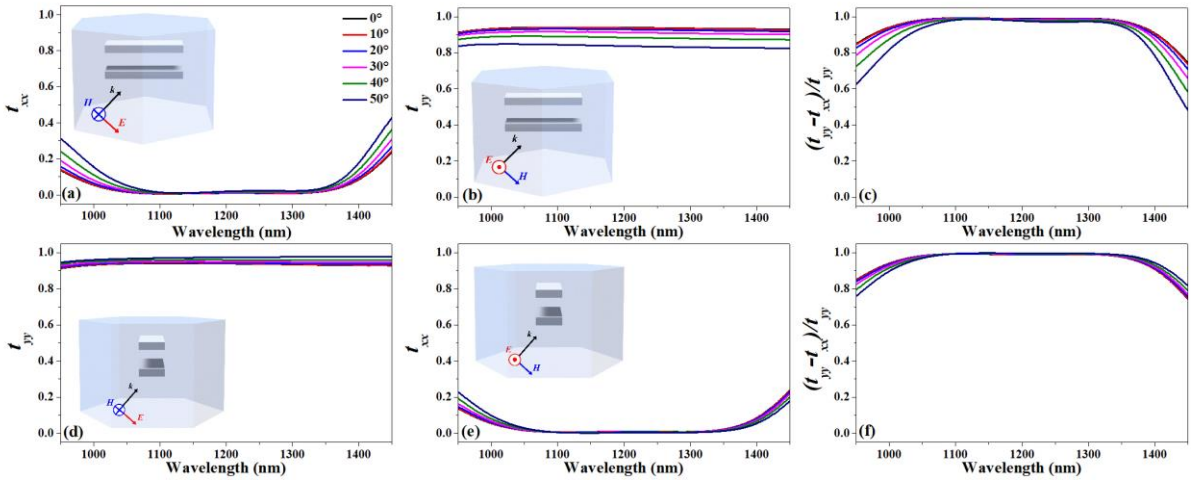

Figure S2. Simulated results of t_{xx} and t_{yy} under illuminations with different incident angles (as the inset shows), the transmission ratio $(t_{yy}- t_{xx})/ t_{yy}$ in (c) is calculated with the simulated results in (a) and (b) while the transmission ratio in (f) is calculated with the simulated results in (d) and (e).

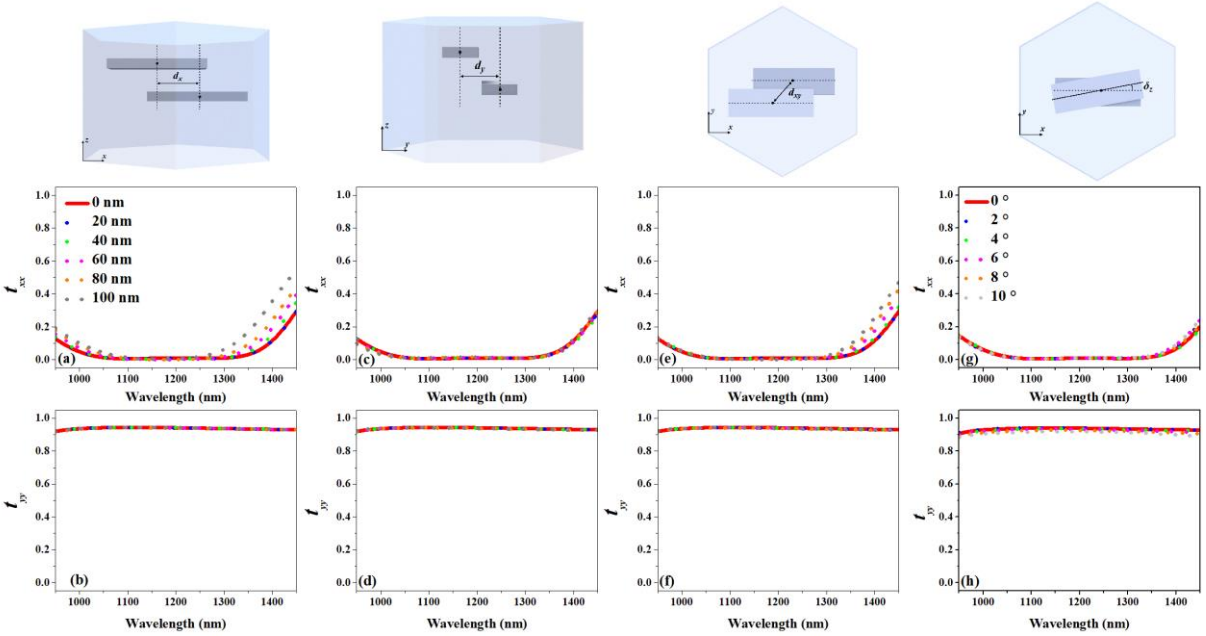

Figure S3. Simulated results of t_{xx} and t_{yy} for bilayer metasurfaces with different misalignment distances along (a) (b) *x*-axis, (c) (d) *y*-axis and (e) (f) both *x*- and *y*-axis and different misalignment angle along (g) (h) *z*-axis.

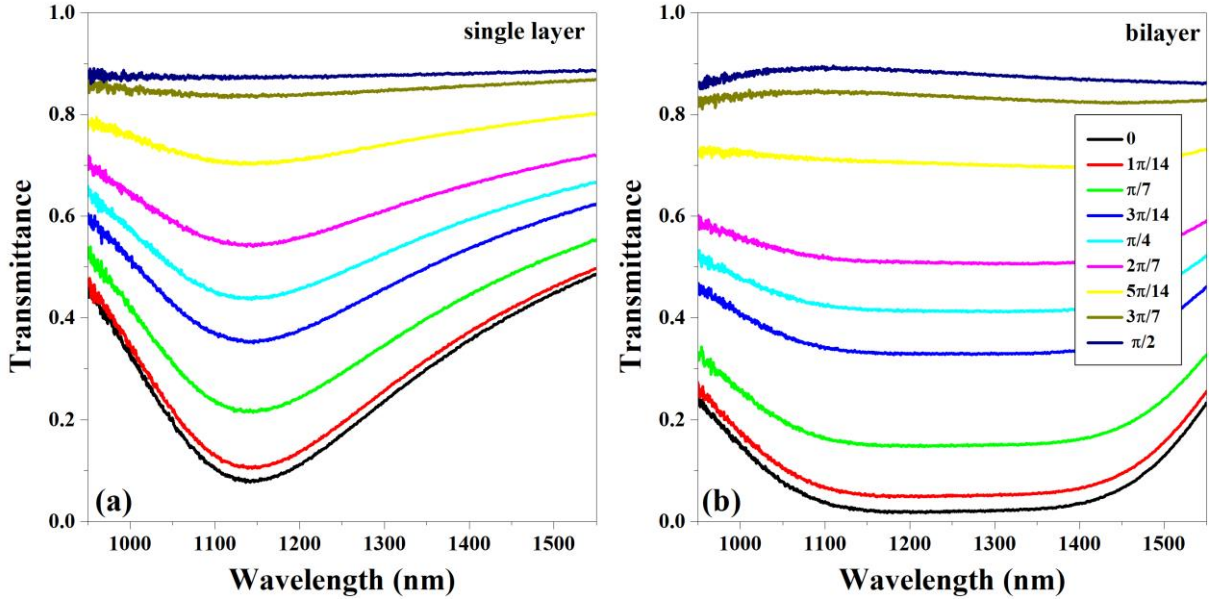

Figure S4. The experimental measurement results of transmittance under linearly polarized illuminations with different polarization angles. (a) Metasurfaces with single layer nanorods and (b) metasurfaces with bilayer nanorods.

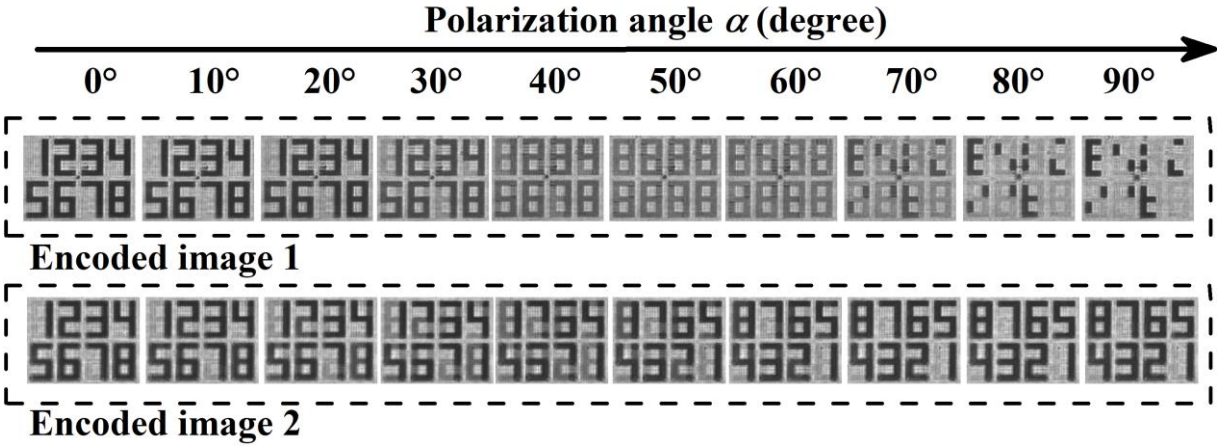

Figure S5. The experimental measurement results of the polarization-encoded images under linearly polarized illumination with different polarization angles. Results confirm that the polarization-encoded image 1 is single outputs and the polarization-encoded image 2 is dual outputs.

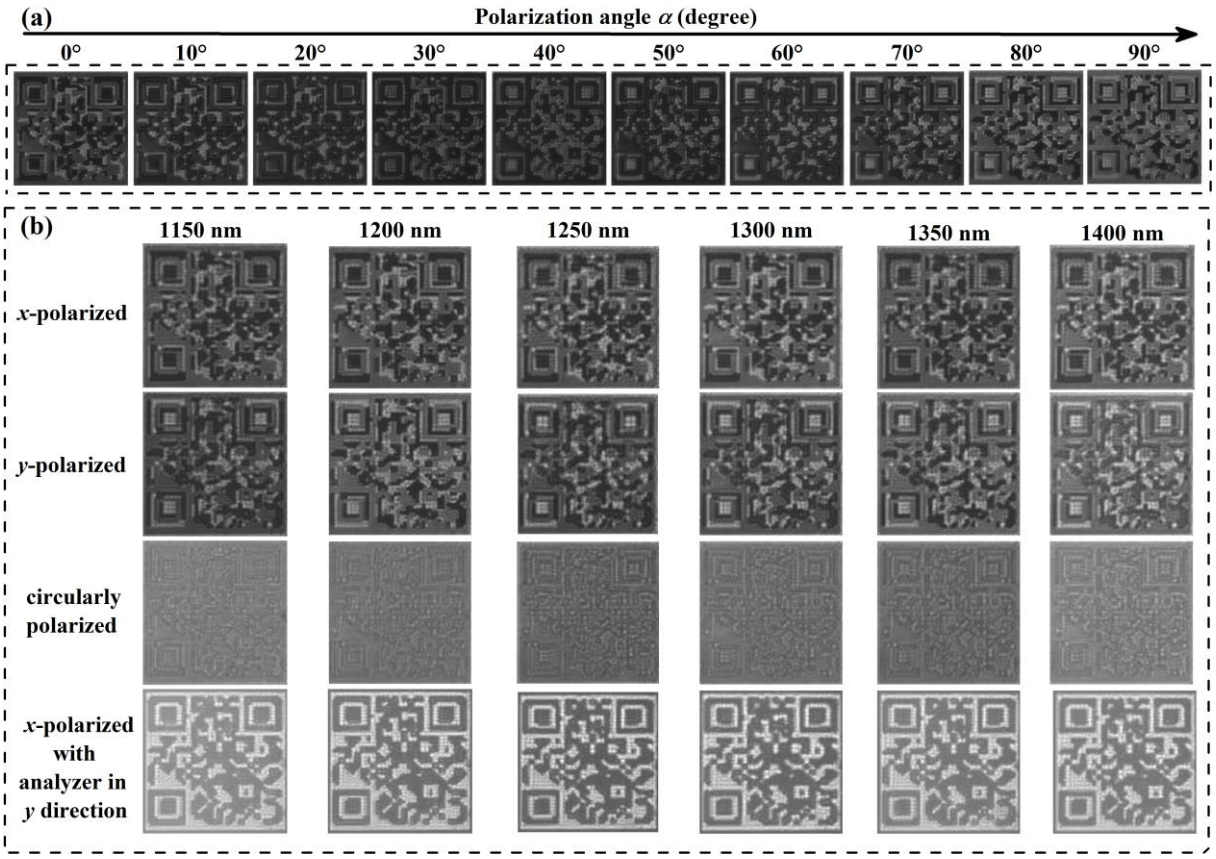

Figure S6. (a) The captured images of the QR code for optical anti-counterfeiting under linearly polarized illumination with different polarization angles. (b) The captured images of the QR code for optical anti-counterfeiting under illumination with different polarization states and wavelengths (the bottom row of images are captured under *x*-polarized illumination with an analyzer in the *y* direction).

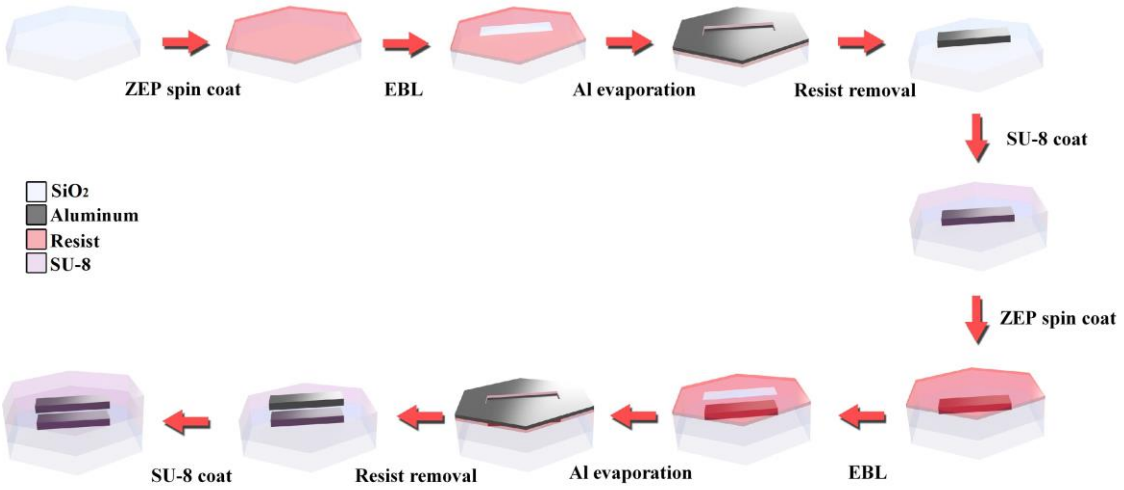

Figure S7. The sample fabrication process of the designed bilayer metasurfaces.

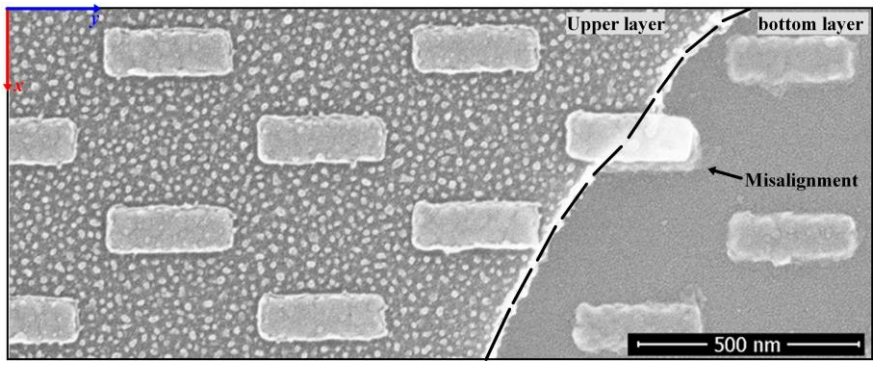

Figure S8. SEM image of the fabricated periodic bilayer metasurface for the verification of the misalignment between the two layers. The orientation angle θ of the nanorods is equal to 90°. In order to see the aluminum nanorods in the upper layer clearly, the SU-8 polymer with thickness approximately equal to 150 nm was etched by oxygen plasma. Then, a very thin platinum was coated on the surface of the sample. However, due to small atomic contrast between Al nanorods and SU-8 and smooth morphology, the aluminum nanorods in the bottom layer could not be seen in the SEM. The white dots in the SEM image come from the etch residue of SU-8 (SU-8 contains antimony which could not be removed by oxygen plasma). To verify the misalignment between the two layers, we removed part of the SU-8 upon the bottom aluminum nanorods by using mechanical method. The etch residues are smaller in the bottom layer because the remained SU-8 is thin after the mechanical removing.

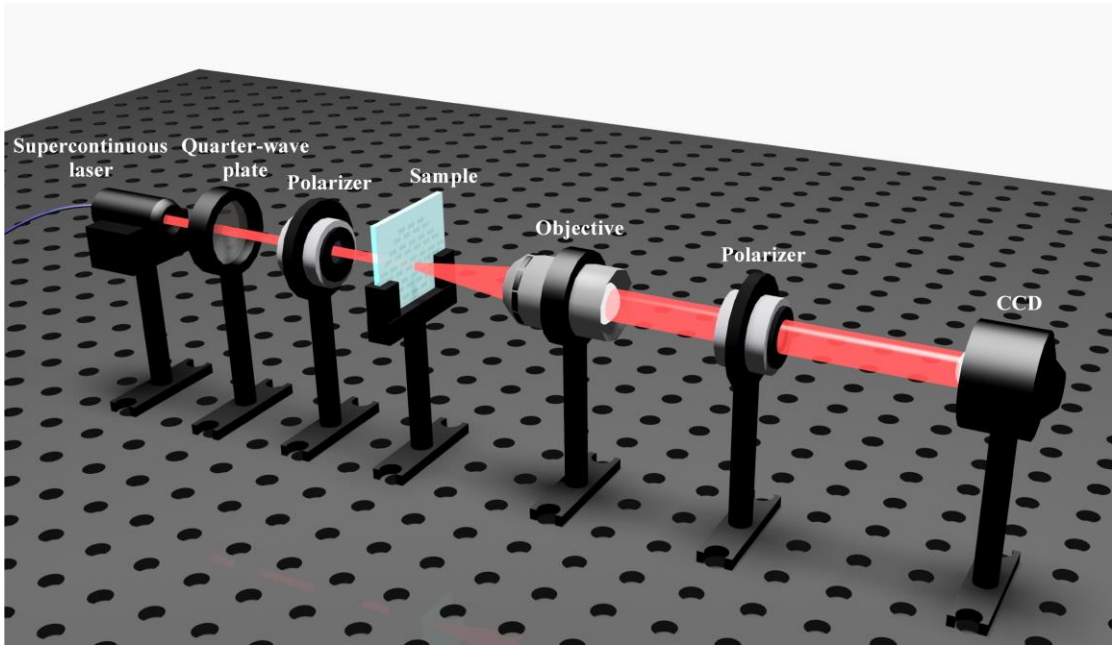

Figure S9. The experimental setup for imaging.

Reference

[S1] N. K. Grady, J. E. Heyes, D. R. Chowdhury, Y. Zeng, M. T. Reiten, A. K. Azad, A. J. Taylor, D. A. R. Dalvit, H.-T. Chen, *Science* **2013**, 1235399.

[S2] J. Liu, Z. Li, W. Liu, H. Cheng, S. Chen, J. Tian, *Adv. Opt. Mater.* **2016**, *4*, 2028-2034.

[S3] H.-T. Chen, *Opt. Express* **2012**, *20*, 7165-7172.